

Premonitory patterns of seismicity months before a large earthquake: Five case histories in Southern California

V. I. Keilis-Borok*^{†‡§}, P. N. Shebalin[†], and I. V. Zaliapin*[‡]

*Institute of Geophysics and Planetary Physics and [†]Department of Earth and Space Sciences, University of California, Los Angeles, CA 90095-1567; and [‡]International Institute for Earthquake Prediction Theory and Mathematical Geophysics, Russian Academy of Sciences, Warshavskoye Shosse, 79, Korpus 2, 113556 Moscow, Russia

Contributed by V. I. Keilis-Borok, October 9, 2002

This article explores the problem of short-term earthquake prediction based on spatio-temporal variations of seismicity. Previous approaches to this problem have used precursory seismicity patterns that precede large earthquakes with “intermediate” lead times of years. Examples include increases of earthquake correlation range and increases of seismic activity. Here, we look for a renormalization of these patterns that would reduce the predictive lead time from years to months. We demonstrate a combination of renormalized patterns that preceded within 1–7 months five large ($M \geq 6.4$) strike-slip earthquakes in southeastern California since 1960. An algorithm for short-term prediction is formulated. The algorithm is self-adapting to the level of seismicity: it can be transferred without readaptation from earthquake to earthquake and from area to area. Exhaustive retrospective tests show that the algorithm is stable to variations of its adjustable elements. This finding encourages further tests in other regions. The final test, as always, should be advance prediction. The suggested algorithm has a simple qualitative interpretation in terms of deformations around a soon-to-break fault: the blocks surrounding that fault began to move as a whole. A more general interpretation comes from the phenomenon of self-similarity since our premonitory patterns retain their predictive power after renormalization to smaller spatial and temporal scales. The suggested algorithm is designed to provide a short-term approximation to an intermediate-term prediction. It remains unclear whether it could be used independently. It seems worthwhile to explore similar renormalizations for other premonitory seismicity patterns.

We consider here a particular approach to earthquake prediction: prediction of large earthquakes based on changes of seismicity in the intermediate magnitude range. The approach we follow here is reviewed in ref. 1. It is focused on well defined prediction algorithms that can be validated by advance prediction. Such a focus is essential both for a fundamental understanding of crustal dynamics and enhancing earthquake preparedness.

Previous studies of observed and modeled seismicity have found a variety of spatio-temporal patterns of medium-magnitude seismicity that emerge as a large earthquake approaches. Well established are “intermediate-term” patterns, which emerge years before a large earthquake and within hundreds of kilometers from the incipient source (2–10, 12–19).[¶] Here, we introduce short-term patterns that emerge with a lead time of months. Our working hypothesis is that some short-term patterns may be defined by renormalization of intermediate-term ones, so that they differ only in the values of adjustable numerical parameters. We consider patterns that reflect two specific premonitory changes of seismicity in the intermediate magnitude range: increases of earthquake correlation range and increases of seismic activity.

Premonitory increases of earthquake correlation range were recognized during the last decade. Several patterns reflecting the rise of correlation range have been suggested (6, 14, 20–24).

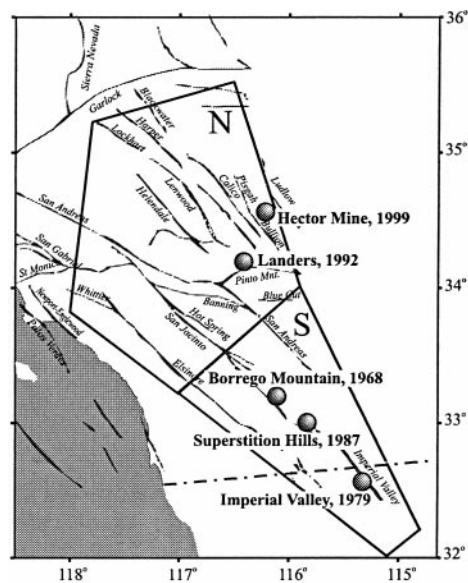


Fig. 1. Area considered for analysis. Circles mark large earthquakes. The area S is considered for earthquakes with $6.4 \leq M < 7$ (the Borrego Mountain, 1968; Imperial Valley, 1979; and Superstition Hills, 1987). The union of areas S and N (SM) is considered for the earthquakes with $M \geq 7$ (Landers, 1992 and Hector Mine, 1999). Fault map after Faults of Southern California, Southern California Earthquake Data Center and ref. 31.

Here we consider two of them, *ROC* (range of correlation) and *Accord*, which were found first in a model (20, 21) and then in observations (22, 23). The pattern *ROC* was observed months before large earthquakes in the Lesser Antilles (22), which makes it especially relevant to the present study.

Increases of seismic activity years to decades before a large earthquake have been well documented during the last century for seismic regions worldwide (2, 5, 12, 13, 15, 17, 18, 25–28). Here, we consider a specific pattern *U* reflecting the rise of seismic activity; it was introduced into earthquake prediction research by Schreider (29).

Data

We use the standard Southern California Seismographic Network earthquake catalog produced by the California Institute of Technology (30). The analysis is carried out within the area shown in Fig. 1 during 1960–2001. Targets for prediction are the five large ($M \geq 6.4$) strike-slip earthquakes listed in Table 1 and marked on Fig. 1.

Abbreviation: ROC, range of correlation.

[§]To whom correspondence should be addressed. E-mail: vkb@ess.ucla.edu.

[¶]Levshina, T. & Vorobieva, I. (1992) *EOS Trans. Am. Geophys. Union* 73, 382 (abstr.).

Table 1. Large earthquakes targeted for prediction

Location	Date	°N, °W	M_L (SCSN)*	M_S (PDE)†
Borrego Mountain	April 9, 1968	33.19, 116.12	6.5	
Imperial Valley	Oct. 15, 1979	32.61, 115.31	6.4	6.9
Superstition Hills	Nov. 24, 1987	33.01, 115.85	6.6	6.6
Landers	June 28, 1992	34.20, 116.43	7.3	7.6
Hector Mine	Oct. 16, 1999	34.59, 116.27	7.1	7.4

*Ref. 30; SCSN, Southern California Seismographic Network.

†PDE, Preliminary Determination of Epicenters, ftp://ghftftp.cr.usgs.gov/pub/pde.

Evolution of seismicity before the large earthquakes is analyzed within the two areas shown in Fig. 1. For the earthquakes with magnitude below 7 (Borrego Mountain, 1968; Imperial Valley, 1979; and Superstition Hills, 1987) we consider the area *S*, which includes the southern reaches of the San Andreas fault network. The union of the areas *S* and *N* (denoted by *SN*) is considered for the larger Landers (1992) and Hector Mine (1999) earthquakes. The area *SN* is the principal plate-boundary fault network of southern California and northwestern Mexico, south of the Garlock fault. The northeastern margin of this area roughly corresponds to the Landers–Mojave earthquake line (32).

The areas considered are chosen in one of many possible ways. This nonuniqueness is also the case with other elements of the subsequent analysis: subdivision of the areas (Fig. 2), the choice of premonitory seismicity patterns, the formalization of these patterns (next section), choosing the values of numerical parameters (Table 2), etc. The influence of these free choices on the prediction results is analyzed in *Stability Test: The Error Diagram*.

Premonitory Seismicity Patterns: Definitions

Previous studies have found a family of premonitory seismicity patterns with common scaling and similar definitions (1). Each of those patterns is captured by a specific functional $F(t)$ defined on a sequence $(t_j, M_j, x_j), j = 1, 2, \dots$ of main shocks within a given area and magnitude range $M_j > m_0$. Here t_j is the occurrence time of the j th main shock, M_j its magnitude, and x_j coordinates of epicenter. The lower magnitude threshold m_0 is determined by the condition $n(m_0) = n_0 \text{ yr}^{-1}$, where $n(M)$ is the average annual number of main shocks with magnitude M or larger, n_0 is an adjustable parameter. The same value of n_0 may correspond to different lower magnitude thresholds due to spatial and temporal variations on the seismic activity; this

Table 2. Adjustable parameters of the prediction algorithm

$n_0, \text{ yr}^{-1}$	$T_R,$ days	C_R	$T_A,$ days	$Q_A, \%$	κ	$C_U, \text{ yr}^{-1}$
20 (40)	10	5	15	99	15	2
15–30 (30–60)	5–30	3–8	7–30	98–99	5–30	0.8–10

Values used in *Patterns ROC, Accord, and U vs. Large Earthquakes* (Figs. 3 and 4) are given in bold. The variation ranges for the stability tests (Fig. 5) are given in plain font. Values of n_0 in brackets refer to the patterns *Accord* and *ROC* within the area *SN*.

dependence introduces self-normalization of premonitory patterns (8, 9). Emergence of the pattern is defined by the condition $F(t) \geq C_F$. The patterns are defined on the earthquake sequence with aftershocks eliminated. The identification of aftershocks is made by the coarse windowing introduced in refs. 33 and 34. For brevity, remaining earthquakes are called the main shocks.

Prediction is targeted at large earthquakes defined by the condition $M_j \geq M_0$. Previous studies suggest that the lower magnitude m_0 of the earthquakes that form premonitory patterns is 3–4 units less than the lower magnitude M_0 of the earthquakes to be predicted (1).

The pattern *ROC* reflects the nearly simultaneous occurrence of medium-magnitude main shocks at large distances (20–22). The functional $R(t)$, which captures this pattern, is defined within a narrow sliding time window $(t - T_R, t)$. It counts the number of pairs (i, j) of main shocks such that $r_{ij} \geq r_0$; here r_{ij} is the distance between the epicenters of the main shocks i and j . The threshold r_0 is normalized by the minimal magnitude M_0 of the earthquakes targeted for prediction: $r_0 = A \cdot 10^{B M_0}$. Such normalization is used in the well established prediction algorithms CN, M8, and SSE (8, 9).[¶] The coefficients are $A = 0.03, B = 0.5$.[¶] We take $M_0 = 6.4$ in the area *S* and $M_0 = 7.0$ in *SN*. Emergence of the pattern *ROC* is defined by the condition $R(t) \geq C_R, C_R$ being an adjustable parameter.

The pattern *Accord* reflects a nearly simultaneous rise of seismic activity in several parts of the area considered (20, 21, 23), hence its name. The area is divided into K sub-areas, and the functional $A(t)$, which captures the pattern, is defined as the number of sub-areas, which have at least one earthquake within a sliding time window $(t - T_A, t)$. This definition is a marginal case of the following general one (20): for each sub-area $k = 1, \dots, K$ its seismic activity is estimated by a chosen measure in a sliding time window. High activity is defined by the condition

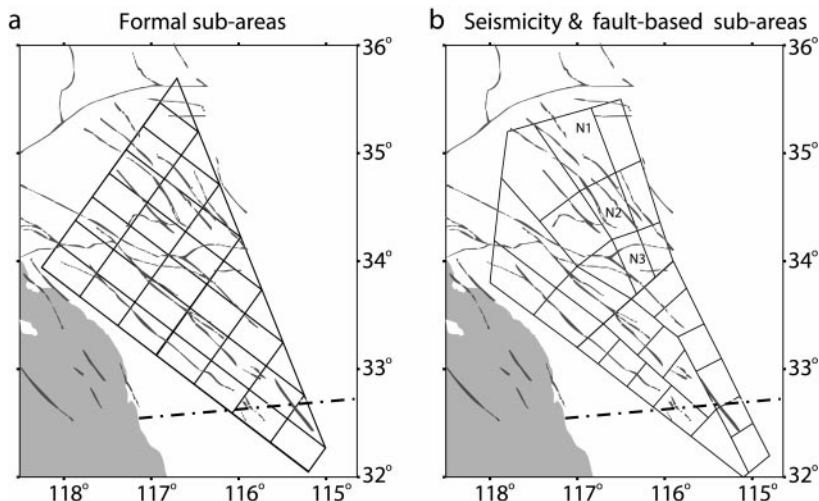


Fig. 2. Divisions into sub-areas by a coarse formal grid (a) and seismicity and fault-based grid (b).

Table 3. Self-adapted thresholds calculated from adjustable parameters

Pattern	Threshold	Large earthquakes				
		Borrego Mountain	Imperial Valley	Superstition Hills	Landers	Hector Mine
<i>ROC</i>	m_0	2.5	3.0	2.9	2.9	3.0
		2.5–2.8	2.9–3.1	2.7–3.0	2.7–3.0	2.7–3.1
	r_0 , km	47	47	47	95	95
<i>Accord</i>	m_0	2.5	3.0	2.9	2.9	3.0
		2.5–2.8	2.9–3.1	2.7–3.0	2.7–3.0	2.7–3.1
	C_A	4	4	4	6	6
<i>U</i>		3–6	3–6	3–6	4–8	4–8
	m_0	2.5	3.0	2.9	3.2	3.3
		2.5–2.8	2.9–3.1	2.7–3.0	3.1–3.3	3.1–3.4

that this measure exceeds a certain threshold. The functional $A(t)$ is defined as the number of the sub-areas where activity is high at the moment t .

Emergence of the pattern *Accord* is defined by the condition $A(t) \geq C_A$. The threshold C_A is adapted to the level of seismicity by a binomial model. Let p be the probability to have at least one main shock within a given sub-area during a time interval T_A . With a uniform distribution of earthquakes, the probability that at least A out of K sub-areas have one or more main shocks is $P(A) = \sum_{a \geq A} p^a (1-p)^{K-a}$ with $p = n_0 T_A K^{-1}$. We chose the threshold C_A as the Q_A percentile of the distribution P .

Seismicity in this model is assumed to be (i) uniformly distributed and (ii) independent in each sub-area. Both of these assumptions lead to overestimation of the probability $P(A)$ for large A , so for high Q_A the functional $A(t)$ exceeds the threshold C_A more rarely than suggested by the model. Thus, we use a reliable lower estimation. Note that the level of seismic activity is used in many earthquake prediction algorithms (1, 2, 4, 5, 7–9, 12–15, 17–19),[†] although for much wider windows than considered here: years instead of weeks.

We consider two alternative divisions into sub-areas. One is a coarse grid oriented along the southern San Andreas fault (Fig. 2a). An advantage of this division is its simplicity and independence of nonunique interpretations of fault maps and seismicity. This simplicity is achieved at the cost of disregarding this potentially relevant information. To use this information we introduce an alternative division (Fig. 2b) where each sub-area roughly corresponds to a relatively large fault. The borders between sub-areas are chosen to avoid dense clouds of epicenters. This division takes into account the fault network and territorial distribution of seismicity at the cost of nonuniqueness in transforming these data into boundaries of sub-areas.

The pattern *U* reflects the increase of the earthquake occurrence rate. It is captured by the functional $U(t_j) = 1/(t_j - t_{j-\kappa+1})$, $j = \kappa, \kappa + 1, \dots$ defined at the occurrence times t_j of main shocks used for analysis. Here the denominator is the length of the minimal time interval, which covers the last κ earthquakes. Emergence of the pattern *U* is defined by the condition $U(t_j) \geq C_U$, C_U being an adjustable parameter.

Patterns *ROC*, *Accord*, and *U* vs. Large Earthquakes

In this section we demonstrate the emergence of the above patterns before the five large earthquakes we consider (see Table 1, Fig. 1). We consider 5-year intervals, each ending at one of the large earthquakes (5 years is a typical lead time for the intermediate-term premonitory seismicity patterns). Analyzing seismicity before the Hector Mine earthquake, we eliminated sub-areas N1, N2, and N3 (Fig. 2b) where activity rose after the

Landers earthquake. Thus we avoided mixing post-Landers activity, decaying but still high, with pre-Hector Mine activity.

Functionals $R(t)$, $A(t)$, and $U(t)$ have been computed with the values of the adjustable parameters indicated in bold in Table 2 and sub-areas shown in Fig. 2b. The corresponding values of the self-adapted thresholds m_0 , r_0 , and C_A calculated from the adjustable parameters are listed in bold in Table 3. They are determined within the time intervals $(t_f - 5 \text{ yr}, t_f - 1 \text{ yr})$, t_f being the moment of a large earthquake. The last year is eliminated from the statistics, since our goal is to find what changed there compared with previous years. For area S we take $n_0 = 20 \text{ yr}^{-1}$, as in the widely used algorithm M8 (8). In the area SN , which contains twice as many sub-areas as S , we take $n_0 = 40 \text{ yr}^{-1}$ for the patterns *ROC* and *Accord*. This procedure ensures that both areas have the same average number of main shocks per sub-area.

Fig. 3 shows the behavior of each functional before the five large earthquakes considered. By definition, a pattern emerges when the functional is equal or larger than the respective threshold (shown by horizontal dotted line in Fig. 3). Patterns emerge sporadically within isolated narrow time intervals. Duration of emergence intervals is up to weeks for patterns *ROC* and *Accord* and up to months for pattern *U*.

The pattern *U* precedes each large earthquake by 2 years or less. Besides, it emerges 4.5 years before the Superstition Hills earthquake. Thus, this pattern still remains an intermediate-term one. At the same time, its lead time is much shorter than 5 years, which is typical for most of the patterns reflecting premonitory rise of activity (1).

The patterns *ROC* and *Accord* precede four large earthquakes (Borrego Mountain, 1968; Imperial Valley, 1979; Landers, 1992; and Hector Mine, 1999) by 3 months or less and the Superstition Hills earthquake by 7 months. These patterns also emerge with a larger (up to 58 months) lead time before the Borrego Mountain, Superstition Hills, and Landers earthquakes. In the previous applications the lead time was also months for *ROC* (22) but it was years for *Accord* (23).

The patterns *ROC* and *Accord* do not seem promising as individual short-term precursors since they would produce many false alarms. Next, we demonstrate that these patterns give better performance when they emerge in the wake of the pattern *U*. To formalize this observation, we formulate the following prediction algorithm:

(i) Whenever the pattern *U* emerges [$U(t) \geq C_U$], a waiting period is declared for the subsequent time interval τ_U .

(ii) When both the patterns *ROC* and *Accord* emerge [$R(t) \geq C_R$ and $A(t) \geq C_A$] during a waiting period, an alarm is declared for the subsequent time interval τ_A .

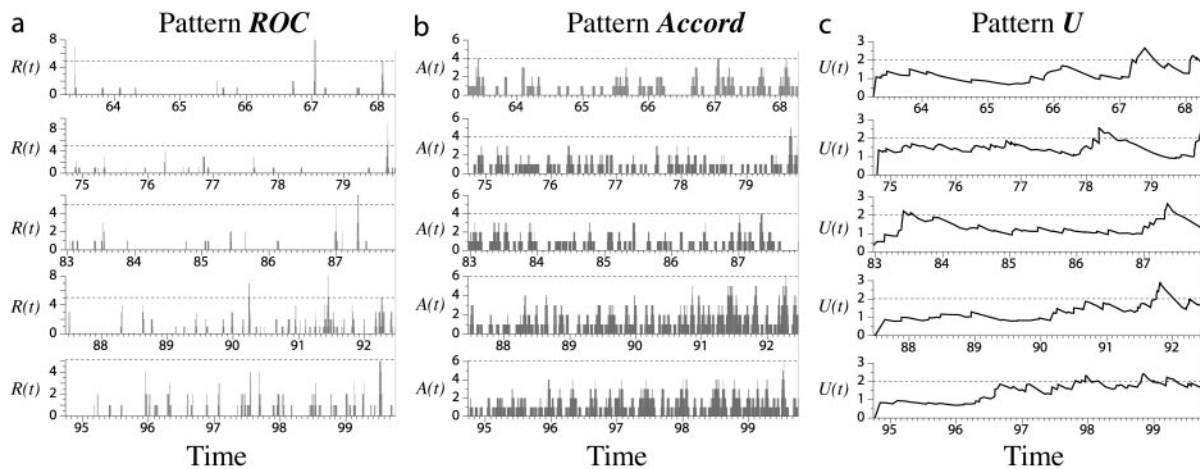


Fig. 3. Individual performance of premonitory patterns. Functionals $R(t)$, $A(t)$, and $U(t)$ during 5-year intervals ending at a large earthquake. The five lines in each panel correspond, from top to bottom, to the large earthquakes in the order of occurrence: Borrego Mountain, 1968; Imperial Valley, 1979; Superstition Hills, 1987; Landers, 1992; and Hector Mine, 1999. Functionals $R(t)$ and $A(t)$, by definition take nonnegative integer values; functional $U(t)$ takes real positive values. Dashed horizontal lines show the thresholds C_U , C_A , and C_R . See details in *Patterns ROC, Accord, and U vs. Large Earthquakes*.

The performance of this algorithm is shown in Fig. 4, which consists of five panels, one for each target earthquake. The top line in each panel shows alarms produced by the algorithm. The dark bars in three bottom lines show emergence intervals of the

patterns *ROC*, *Accord*, and *U*. Notable is the temporal correlation between the patterns, particularly *ROC* and *Accord*. Waiting periods declared after the emergence of the pattern *U* are marked by light shadowing. Parameters of the functionals $R(t)$,

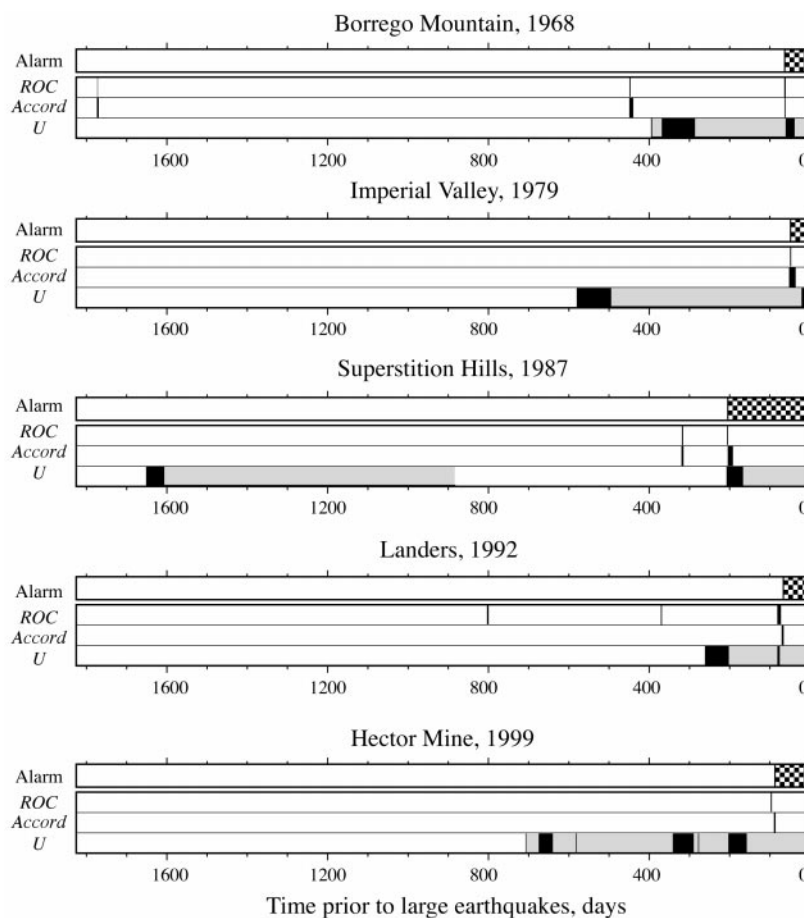


Fig. 4. Short-term alarms. Each panel shows a 5-year interval ending with a large earthquake. The top line shows (by checkered bars) the alarms retrospectively determined by the algorithm. The three lower lines correspond to premonitory patterns indicated at the left. Dark bars show the time intervals when a pattern emerges. Light bars in the bottom line mark waiting periods.

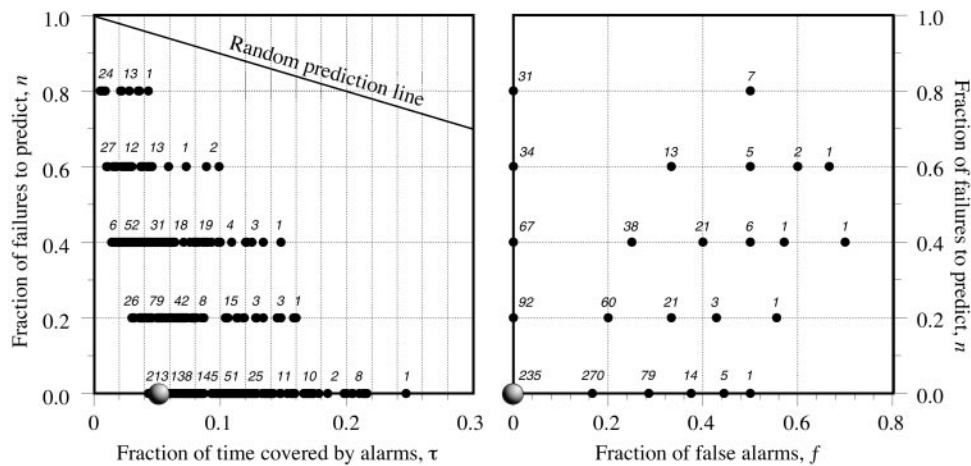


Fig. 5. Error diagram. The diagram compares performance of the prediction algorithm for 1,008 sets of its adjustable elements (see definition in *Stability Test: The Error Diagram*). Values $n = 0.2, 0.4$, etc. correspond to $N_f = 1, 2$, etc. failures to predict. Interval 0.1 on the τ scale is 30 months (6 months per large earthquake). Numbers on the right show how many sets correspond to a given (f, n) combination. Numbers on the left show how many sets correspond to a given value of n and interval of τ . The line $n + \tau = 1$ shown (*Left*) corresponds to a random binomial prediction: alarm is declared at each time step with probability τ . Note the stability of performance: 235 (23%) variants predict all five earthquakes with no false alarms (an example marked by the large circle is shown in Fig. 4); 270 (26%) variants predict all five earthquakes with one false alarm; 92 (9%) variants predict four earthquakes with no false alarm.

$A(t)$, and $U(t)$ are the same as in Fig. 3, $\tau_U = 24$ months and $\tau_A = 7$ months. The resulting lead times between the declaration of an alarm and the subsequent large earthquake vary from 49 to 205 days.

Fig. 4 might suggest an alternative algorithm, based on the fact that all three patterns emerge in arbitrary order within 7 months before a large earthquake. What would be the outcome of this alternative algorithm? Generally, what would be the outcome of prediction if we vary each of its adjustable elements? We answer this question in the next section by exploring a wide range of possible alternatives.

Stability Test: The Error Diagram

Here, we evaluate the stability of our algorithm: vary its adjustable elements, repeat prediction, and compare the results on an error diagram. The error diagram was introduced into seismological studies by G. Molchan (35); its definition follows.

Consider a prediction algorithm applied on a certain territory during the period T years. Suppose that A alarms are declared and A_f of them are false. N strong earthquakes occurred and N_f of them are not covered by alarms (unpredicted). The alarms cover altogether the time D year. Performance of the algorithm is characterized by three dimensionless errors: the relative duration of alarms, $\tau = D/T$; the fraction of failures to predict, $n = N_f/N$; and the fraction of false alarms, $f = A_f/A$. The error diagram shows the values of τ , n , and f for different versions of a prediction algorithm.

We have considerably varied the adjustable elements of the algorithm. In particular, we have tested four alternative rules for alarm declaration based on interplay of the three individual patterns; four versions of sub-areas (used to define the pattern *Accord*) of different size and orientation; and a wide range of adjustable numerical parameters varied uniformly within the ranges indicated in the second line of Table 2. The corresponding ranges of self-adapted thresholds m_0 , r_0 , and C_A are indicated in Table 3. Note that the wide ranges of variation for the parameter n_0 (say, from 15 to 30 in area S) correspond to modest ranges of variation for the magnitude threshold m_0 (typically, 0.3 units of magnitude).

Altogether we have considered >1,000 sets of algorithm's adjustable elements. Prediction was done with each of them; the results are juxtaposed in the error diagram of Fig. 5. The error

diagram shows that prediction performance is reasonably stable: 23% of the versions considered predict all five large earthquakes with no false alarms (corresponding points lie at the origin of the error diagram), and 60% give the error score $A_f + N_f \leq 1$ (no more than one false alarm or one unpredicted earthquake). Parameters corresponding to these predictions fill a reasonably wide domain in the parameter space. The average duration of alarms is shorter than 5 months per earthquake. The limits where the good performance fails (say, correspond to $A_f + N_f \geq 3$) are reached in 20% of the versions. Other results may be summed up as follows:

- (i) The most stable is prediction of the Landers earthquake, which is predicted by 94% of the variants considered; the least stable is prediction of the Borrego Mountain earthquake (79%).
- (ii) Important for our prediction is the spatial scale of the sub-areas (20–50 km) and not a particular position of borders. This notion is supported by the fact that formal sub-areas (Fig. 2a) and those based on the fault map and seismicity (Fig. 2b) give similar performance.
- (iii) The rise of activity (pattern U) and rise of correlation range (patterns *ROC* and *Accord*) indeed play different roles in the transition to a large earthquake. This finding is supported by the fact that the prediction rule suggested earlier (uniform use of the individual patterns) gives more errors than the rules that use *ROC* and *Accord* differently from U .

More details are given in Table 4 and *Supporting Text*, which are published as supporting information on the PNAS web site, www.pnas.org.

Discussion

We renormalized in time and space three previously known premonitory seismicity patterns, which reflect the increase of seismic activity and increase of earthquake correlation range. A combination of the renormalized patterns provides, in retrospect, a short-term prediction (with lead time of months) of the five largest earthquakes in Southeastern California, including the Landers and Hector Mine earthquakes.

What Is a Possible Physical Interpretation of a Premonitory Earthquake Sequence Introduced Here? Rise of earthquake correlation range indicates that the blocks surrounding a soon-to-break fault start to aggregate, tending to move as a whole. The pattern

Accord captures this phenomenon on a relatively high level of averaging. The pattern *ROC* captures this phenomenon without any spatial averaging, by the emergence of individual earthquakes. The displacement rate should be sufficiently large, which is ensured by the general rise of seismic activity (pattern *U*).

These processes are not permanent; they are realized in sporadic episodes reflected by distinct peaks of the functionals. Each peak lasts for weeks (patterns *ROC* and *Accord*) or months (pattern *U*). Similar irregularity on a larger scale is exhibited by the intermediate-term patterns.

Why Renormalization? It can be naturally explained by the phenomenon of self-similarity, a general feature of many nonlinear systems. Such systems exhibit well defined behavior patterns (36–38), which emerge in similar form on different scales. Generally, the renormalization to short-term scales is well explored in the modeling of critical transitions, although not in connection with prediction problem (39–44). If our results reflect reality, the premonitory patterns we analyzed exhibit a specific kind of similarity: they retain their predictive power in different spatio-temporal scales.

Further Tests. Exhaustive retrospective tests show that the suggested algorithm is reasonably stable to variations of its adjustable elements (numerical parameters being only part of them). This finding encourages its further test in other regions. Such tests are facilitated by the fact that the algorithm is self-adapting to the level of background seismicity. Results of such tests for other parts of California, the Eastern Mediterranean, and Japan will be published elsewhere.

Transition from Intermediate- to Short-Term Prediction? By definition, our algorithm can be used as a second approximation to an intermediate-term one, which would provide initial alarms within several hundred kilometers and several years. It remains unclear whether our algorithm can be used independently.

A consecutive approximation approach was pioneered with singular success in prediction of the Haicheng earthquake in China in 1975 (28). Kossobokov *et al.* (45) describe a premonitory short-term rise of activity in areas of intermediate-term alarms of the algorithm MSc in the Pacific Rim and California.

What Do We Rely On? The quest for short-term earthquake precursors has been less than successful so far. A multitude of such precursors have been suggested over the decades, but hardly any were validated by systematic applications, with a reproducible count of errors and successes. Many current efforts are focused on electromagnetic precursors (11). Our hope rests on taking advantage of the following previous findings: extents of averaging of seismicity in time and space; normalized self-adapting definitions; the recently introduced patterns, which reflect increase of earthquake correlation range; and a consecutive approximation approach.

We are grateful to D. Turcotte, L. Knopoff, A. Gabrielov, and G. Axen for insightful, hard, and constructive criticism. G. Axen provided invaluable consultations about geological description of the areas considered. This study was supported by The 21st Century Collaborative Activity Award for Studying Complex Systems from the James S. McDonnell Foundation.

- Keilis-Borok, V. I. (2002) *Annu. Rev. Earth Planet. Sci.* **30**, 1–33.
- Keilis-Borok, V. I. & Malinovskaya, L. N. (1964) *J. Geophys. Res.* **B 69**, 3019–3024.
- Keilis-Borok, V. I., Knopoff, L. & Rotwain, I. M. (1980) *Nature* **283**, 258–263.
- Wyss, M. & Habermann, R. E. (1987) *U.S. Geol. Surv. Open-File Rep.* **2**, 526–536.
- Knopoff, L., Levshina, T., Keilis-Borok, V. I. & Mattoni, C. (1996) *J. Geophys. Res.* **B 101**, 5779–5796.
- Prozorov, A. G. & Schreider, S. (1990) *Pure Appl. Geophys.* **133**, 329–347.
- Keilis-Borok, V. I., ed. (1990) *Phys. Earth Planet. Int.* **61**, 1–144.
- Keilis-Borok, V. I. & Kossobokov, V. G. (1990) *Phys. Earth Planet. Int.* **61**, 73–83.
- Keilis-Borok, V. I. & Rotwain, I. M. (1990) *Phys. Earth Planet. Int.* **61**, 57–72.
- Molchan, G. M., Dmitrieva, O. E., Rotwain, I. M. & Dewey, J. (1990) *Phys. Earth Planet. Int.* **61**, 128–139.
- Uyeda, S. & Park, S., eds. (2002) *J. Geodyn.* **33**, 377–570.
- Varnes, D. J. (1989) *Pure Appl. Geophys.* **130**, 661–686.
- Bufe, C. G. & Varnes, D. J. (1993) *J. Geophys. Res.* **B 98**, 9871–9883.
- Kossobokov, V. G. & Carlson, J. M. (1995) *J. Geophys. Res.* **B 100**, 6431–6441.
- Press, A. & Allen, C. (1995) *J. Geophys. Res.* **B 100**, 6421–6430.
- Rotwain, I., Keilis-Borok, V. & Botvina, L. (1997) *Phys. Earth Planet. Int.* **101**, 61–71.
- Bowman, D. D., Ouillon, G., Sammis, C. G., Sornette, A. & Sornette, D. (1998) *J. Geophys. Res.* **B 103**, 24359–24372.
- Jaume, S. C. & Sykes, L. R. (1999) *Pure Appl. Geophys.* **155**, 279–306.
- Keilis-Borok, V. & Shebalin, P. N., eds. (1999) *Phys. Earth Planet. Int.* **111**, 179–330.
- Gabrielov, A. M., Zaliapin, I. V., Newman, W. I. & Keilis-Borok, V. I. (2000) *J. Geophys. Int.* **143**, 427–437.
- Zaliapin, I., Keilis-Borok, V. I. & Ghil, M. (2001) *J. Stat. Phys.*, in press.
- Shebalin, P., Zaliapin, I. & Keilis-Borok, V. (2000) *Phys. Earth Planet. Int.* **122**, 241–249.
- Zaliapin, I., Keilis-Borok, V. I. & Axen, G. (2002) *J. Geophys. Res.*, in press.
- Zoeller, G., Hainzl, S. & Kurths, J. (2001) *J. Geophys. Res.* **B 106**, 2167–2176.
- Gutenberg, B. & Richter, C. F. (1954) *Seismicity of the Earth and Associated Phenomena* (Hafner, New York).
- Tocher, D. (1959) *Calif. Div. Mines Spec. Rep.* **57**, 39–48.
- Shaw, B. E., Carlson, J. M. & Langer, J. S. (1992) *J. Geophys. Res.* **B 97**, 479–488.
- Ma, Z., Fu, Z., Zhang, Y., Wang, C., Zhang, G. & Liu, D. (1990) *Earthquake Prediction: Nine Major Earthquakes in China* (Springer, New York).
- Shreider, S. (1999) *Phys. Earth Planet. Int.* **61**, 113–127.
- Southern California Seismographic Network (1932–2002) *Southern California Seismographic Network Format Catalog Data* (California Institute of Technology, Pasadena), www.scecdc.seec.org/ftp/catalogs/SCSN.
- Jennings, C. W. (1994) *Fault Activity Map of California and Adjacent Areas, Scale 1:750,000* (Department of Conservation, Division of Mines and Geology, Sacramento, CA).
- Nur, A., Hagai, R. & Beroza, G. C. (1993) *Science* **261**, 201–203.
- Gardner, J. & Knopoff, L. (1974) *Bull. Seismol. Soc. Am.* **64**, 1363–1367.
- Keilis-Borok, V., Knopoff, L., Rotwain, I. & Sidorenko, T. (1980) *J. Geophys. Res.* **B 85**, 803–811.
- Molchan, G. M. (1997) *Pure Appl. Geophys.* **149**, 233–247.
- Gell-Mann, M. (1994) *The Quark and the Jaguar: Adventures in the Simple and the Complex* (Freeman, New York).
- Holland, J. H. (1995) *Hidden Order: How Adaptation Builds Complexity* (Addison-Wesley, Reading, MA).
- Gunderson, L. H. & Holling, C. S., eds. (2001) *Panarchy: Understanding Transformations in Human and Natural Systems* (Island, Washington, DC).
- Allegre, C. J., Lemouel, J. L. & Provost, A. (1982) *Nature* **297**, 47–49.
- Newman, W. I., Gabrielov, A. & Turcotte, D. L., eds. (1994) *Nonlinear Dynamics and Predictability of Geophysical Phenomena: Geophysical Monograph Series 83* (Am. Geophys. Union, Washington, DC).
- Newman, W. I., Turcotte, D. L. & Gabrielov, A. (1995) *Phys. Rev. E Stat. Phys. Plasmas Fluids Relat. Interdiscip. Top.* **52**, 4827–4835.
- Rundle, B. J., Turcotte, D. L. & Klein, W., eds. (2000) *Geocomplexity and the Physics of Earthquakes* (Am. Geophys. Union, Washington, DC).
- Turcotte, D. L. (1997) *Fractals and Chaos in Geology and Geophysics* (Cambridge Univ. Press, Cambridge, U.K.), 2nd Ed.
- Sornette, D. & Sammis, C. G. (1995) *J. Phys.* **I 5**, 607–619.
- Kossobokov, V. G., Keilis-Borok, V. I., Romashkova, L. L. & Healy, J. H. (1999) *Phys. Earth Planet. Int.* **111**, 187–196.

Supporting Text

Stability Analysis. The following variations of the algorithm have been considered.

Definition of the algorithm:

a) In rule *ii* the condition “...both the patterns *ROC* and *Accord* emerge...” is replaced by the weaker condition, “...pattern *ROC* or *Accord* emerges...”

b) Rule *ii* is changed: an alarm is declared when patterns *ROC* and *Accord* emerge not only after the emergence of the pattern *U* but also within Δ days before it.

c) The three patterns considered are used in a uniform way: whenever either pattern emerges, a waiting period is declared for a subsequent time interval $\tau_{RAU} = 7$ months. An alarm is the intersection of the three waiting periods triggered by each pattern.

d) Alternative normalization of the threshold r_0 in the pattern *Accord*: r_0 is defined as the Q_R percentile of the r_{ij} distribution.

Division into sub-areas:

e) Four different versions of areas and sub-areas are considered. They include variation of the size (from 20 to 50 km) and orientation of the sub-areas.

f) The territory activated by the Landers earthquake was not eliminated from seismicity preceding the Hector Mine earthquake.

Adjustable numerical parameters:

g) Variations are indicated in plain font in Table 2.

Next, we describe in detail the prediction performance corresponding to described variations of the adjustable elements of the algorithm. This might provide insight for a reader interested in the development of alternative algorithms. The letters in italics refer to the variations described above.

(i) All the target earthquakes are predicted with no false alarms by 23% of the versions considered. This includes: different rules for alarm declaration (*a-c*); different definitions of r_0 (*d*); variations of areas and sub-areas (*e*), retaining the area of activation after the Landers earthquake (*f*); and, finally, a considerable variation of numerical parameters (*g*): n_0 ranges from 17.5 to 22.5; T_R from 5 to 30 days; C_R from 3 to 8; T_A from 7 to 30 days; both distinct values of Q_A , 98% and 99%; κ from 10 to 25, C_U from 1.0 to 4.0 yr^{-1} .

(ii) One false alarm or one failure to predict is obtained for 36% of the versions. This includes the variations indicated in *i*, and broader limits for n_0 (15-25), κ (5-30), and C_U (0.8 to 10.0 yr^{-1}).

(iii) Two errors are obtained for 21% of the versions.

(iv) Failure of performance (three to seven errors) is reached for the remaining 20% of the versions.

(v) To sustain zero failures to predict is easier than zero false alarms: 58% of variations have no failures to predict with two or fewer false alarms; and only 39% have the opposite relation, no false alarms and two or fewer failures to predict.

Statistics of errors with different definitions of alarms and different divisions into sub-areas is summarized in Table 4.

Table 4. Statistics of errors for different versions of the algorithm (in %)

Version of the algorithm	0 error	1 error	2 errors	No false alarms at 0-2 failures to predict	No failures to predict at 0-2 false alarms
Alarm definition					
Rule $A \& R$	30	62	80	60	49
Rule $A R$	24	63	84	31	72
Rule $A \& R \& U$	1	13	67	11	42
Rule $A \& R$					
$\tau_U = 24$ months, $\Delta = 0$	27	63	80	49	56
$\tau_U = 24$ months, $\Delta = 1.5$ months	27	66	81	53	51
$\tau_U = 3$ months, $\Delta = 1.5$ months	38	57	79	70	42
Rule $A R$					
$\tau_U = 24$ months, $\Delta = 0$	8	60	83	11	76
$\tau_U = 24$ months, $\Delta = 1.5$ months	28	67	86	34	74
$\tau_U = 3$ months, $\Delta = 1.5$ months	35	63	83	47	66
Areas and sub-areas					
Formal grid	15	55	77	31	54
Seismicity & fault-based grid	31	63	80	47	61

We see that both the $A \& R$ and $A | R$ rules give about the same total count of errors. By definition, the first rule gives relatively more failures to predict, and fewer false alarms. Rule $A \& R \& U$ gives more alarms of both kinds. The three combinations of τ_U and Δ also give a similar overall performance, i.e. 80-85% of cases with two or fewer errors. The rule $A \& R$ with a short waiting time $\tau_U = 3$ months, $\Delta = 1.5$ months gives the largest number of predictions with no false alarms and zero to two failures to predict. With a long waiting time, $\tau_U = 24$ months, the score reverses to no failures to predict and zero to two false alarms. Using similar tables as above, we studied the variation of each adjustable numerical parameter. The algorithm naturally is most sensitive to the variation of the parameter n_0 that participates in the definition of all the three patterns, scaling the lower magnitude cutoff and the thresholds C_A . Larger values increase the number of false alarms, smaller values increase the number of failures to predict. Different definitions of the threshold r_0 in general give similar total rate of errors, except for a few marginal cases. Parameter T_R is also not critical: additional errors are often easily compensated for by the change of the threshold C_R . The value $T_R = 10$ days gives more stable results than $T_R = 7$ days, used initially. Variation of the parameter T_A does not affect the rate of errors much, partly because the changes are balanced by the self-adapting parameter C_A . Values of 15 and 20 days are a little better than others. The value $Q_A = 0.99$ gives on average a

better performance. The parameter κ (used in the definition of the pattern U) gives similar performance in the range from 10 to 20, with proportional change of the threshold C_U . This corroborates the initial choice $\kappa = 15$.